



# Preparation and evaluation of new pyridone derivatives and their investigation corrosion depletion property for copper corrosion in HCl acid solution

Badreah A. Al Jahdaly<sup>1</sup>

Received: 6 November 2022 / Revised: 3 January 2023 / Accepted: 4 January 2023 / Published online: 28 January 2023  
© The Author(s), under exclusive licence to Springer-Verlag GmbH Germany, part of Springer Nature 2023

## Abstract

The present research aimed to investigate the impact of some synthetic derivatives of pyridone (6-amino-1-(4-hydroxyphenyl)-4-(4-methoxyphenyl)-2-oxo-1,2-dihydropyridine-3,5-dicarbonitrile (PYR-2) and 6-amino-1-(4-hydroxyphenyl)-2-oxo-4-phenyl-1,2-dihydropyridine-3,5-dicarbonitrile (PYR-3)) on copper corrosion inhibition behavior in HCl acid solution using electrochemical methods, including potentiodynamic polarization (PP) and electrochemical impedance spectroscopy (EIS). Using FTIR, <sup>1</sup>HNMR, and mass spectroscopy methods, the two compounds ((PYR-2) and (PYR-3)) were confirmed and characterized. With the two compounds added to corrosive media, the double-layer capacitance value decreases. In the case of  $18 \times 10^{-5}$  M, they reached maximum efficiency of 91.9% and 90.3%, respectively. Having studied its behavior during adsorption on copper, it was concluded that it follows chemical adsorption and Langmuir isotherm and may be considered mixed-type inhibitors.

**Keywords** Corrosion inhibition · Copper · HCl · Pyridone derivatives · Langmuir isotherm

## 1 Introduction

There are many uses for copper in different industries because it is an ideal conductor of electricity and heat and has other properties that make it a perfect mineral for use in various fields [1]. Copper is usually cleaned with acids to produce its properties as efficiently as possible, which causes corrosion of its surface, resulting in heavy economic losses [2]. Organic compounds are among the most effective ways of protecting from corrosion [3, 4]. These compounds adsorb to the surface of metals, which inhibits anodic and cathodic processes, thereby reducing metal dissolution. Besides deterioration in acidic media and hydrogen gas formation, copper has high positive potential because of its high corrosion resistance [5, 6]. By removing dissolved oxygen from acidic media, copper can be protected. Various researches yielded a good number of organic compounds used as corrosion inhibitors owing to the existence of N, S, and O atoms

and double bonds in them. Heterocyclic compounds are the most important of these compounds. Recently, heterogeneous organic compounds containing N, S, and O atoms have occupied the interest of researchers to find copper corrosion inhibitors in various acid solutions. These compounds are of great interest due to their adsorption properties and the creation of an oxide layer on the metal surface [7, 8].

Additionally, we need to consider the presence of benzene radicals, the charge density, the molecular weight of the inhibitors, and the type of adsorption when choosing an inhibitor. Among the many compounds of essential origin [9] containing the 2-pyridone structure, many possess biological activity, making their derivatives particularly potent as antibacterial and antifungal [10, 11]. There are many applications for 2-pyridone derivatives, including paints, pigments, fuel and lubricant additives, acid–base indicators, and stabilizers for polymers and coatings [12, 13]. The novelty of our study aimed to develop new and effective copper corrosion inhibitor compounds in HCl. Two pyridone inhibitors (6-amino-1-(4-hydroxyphenyl)-4-(4-methoxyphenyl)-2-oxo-1,2-dihydropyridine-3,5-dicarbonitrile (PYR-2) and 6-amino-1-(4-hydroxyphenyl)-2-oxo-4-phenyl-1,2-dihydropyridine-3,5-dicarbonitrile (PYR-3)) were used in our research. Electrochemical

✉ Badreah A. Al Jahdaly  
bajahdali@uqu.edu.sa

<sup>1</sup> Chemistry Department, Faculty of Applied Science, Umm Al-Qura University, Makkah, Saudi Arabia

methods such as PP and EIS were employed to confirm their efficiency in blocking adsorption by investigating the kind and mode of adsorption on the copper surface. Density functional theory calculations and Monte Carlo simulations were also used to support the experimental findings.

## 2 Experimental

### 2.1 Materials

Copper samples were utilized to conduct experiments, which were injected in Teflon, and the gap between the surface of the copper and Teflon was filled with epoxy. Saturated calomel (SCE), platinum (Pt) sheet, and as a counter, reference, and working electrode, copper metal was used. AnalaR grade of HCl (35%) was diluted with bi-distilled water to prepare corrosive solutions.

### 2.2 Inhibitors preparation

#### 2.2.1 Synthesis of 6-amino-1-(4-hydroxyphenyl)-4-(4-methoxyphenyl)-2-oxo-1,2-dihydropyridine-3,5-dicarbonitrile (PYR-2)

6-amino-1-(4-hydroxyphenyl)-4-(4-methoxyphenyl)-2-oxo-1,2-dihydropyridine-3,5-dicarbonitrile to a solution of the 2-(4-methoxybenzylidene)malononitrile (0.36 g, 2 mmol) in EtOH (20 mL) was added the acetamide 1 (0.35 g, 2 mmol). The heat was applied to the reaction mixture, which included a few drops of piperidine, and it remained in this state, under reflux, for 2 h. A pale yellow powder with a yield of 87% and a melting point (m.p) of 212–215 °C were obtained after collecting the solid product via filtering, washing it with EtOH, and crystallizing it from (3:1) absolute ethanol: DMF mixture.

#### 2.2.2 Synthesis of 6-amino-1-(4-hydroxyphenyl)-2-oxo-4-phenyl-1,2-dihydropyridine-3,5-dicarbonitrile (PYR-3)

The acetamide 1 (0.35 g, 2 mmol) and a few piperidine drops were added to a 2-benzylidene malononitrile solution (0.30 g, 2 mmol) in EtOH (20 mL) as shown in Fig. 1. For 2 h, the reaction mixture was subjected to reflux heating. The solid product was filtered, rinsed with EtOH, and crystallized from an ethanol/DMF solution, (4:1) mixture to obtain a pale yellow powder with 85% purity and an m.p of 212–215 °C.

### 2.3 Electrochemical tests

Before the quasi-steady state can be studied, the copper electrode must first be dipped in hydrochloric acid at the open-circuit voltage (OCP). Using frequencies of  $10^5$ – $10^{-2}$  Hz and an AC sine wave of 10 mV at (OCP), the (EIS) results were conducted [14, 15]. Next, the following equation was used to determine the efficiency of the two compounds:

$$\eta\% = 0 \times 100 = \left( \frac{R_{ct} - R_{ct}^{\circ}}{R_{ct}} \right) \times 100 \quad (1)$$

$R_{ct,0}$  and  $R_{ct}$  are charge-transfer resistances of uninhibited and inhibited copper, respectively. In addition to  $E_{OCP}$ , the PP was conducted at 0.2 mV/s within a  $\pm 250$  mV concerning corrosion potential. Our relevant  $\eta$  values were computed by employing the equation:

$$\eta\% = 0 \times 100 = \left( \frac{i_{corr}^{\circ} - i_{corr}}{i_{corr}^{\circ}} \right) \times 100 \quad (2)$$

$i_{corr,0}$  and  $i_{corr}$  mean current density values in the lack and the existence of the protection of compounds, respectively. With a computer monitor attached to Potentiostat/Galvanostat/ZRA, a Gamry framework system based on the ESA 400 is included. Gamry applications include the DC105 polarization software and the EIS300 EIS program. For charting, graphing, and fitting data, the Echem Analyst 6.03 program was used. All the tests carried out at R.T. Triplicate experiments were performed under identical conditions to ensure the consistency of the results. Before beginning any measurements, the electrode potential to was waited 30 min to settle.

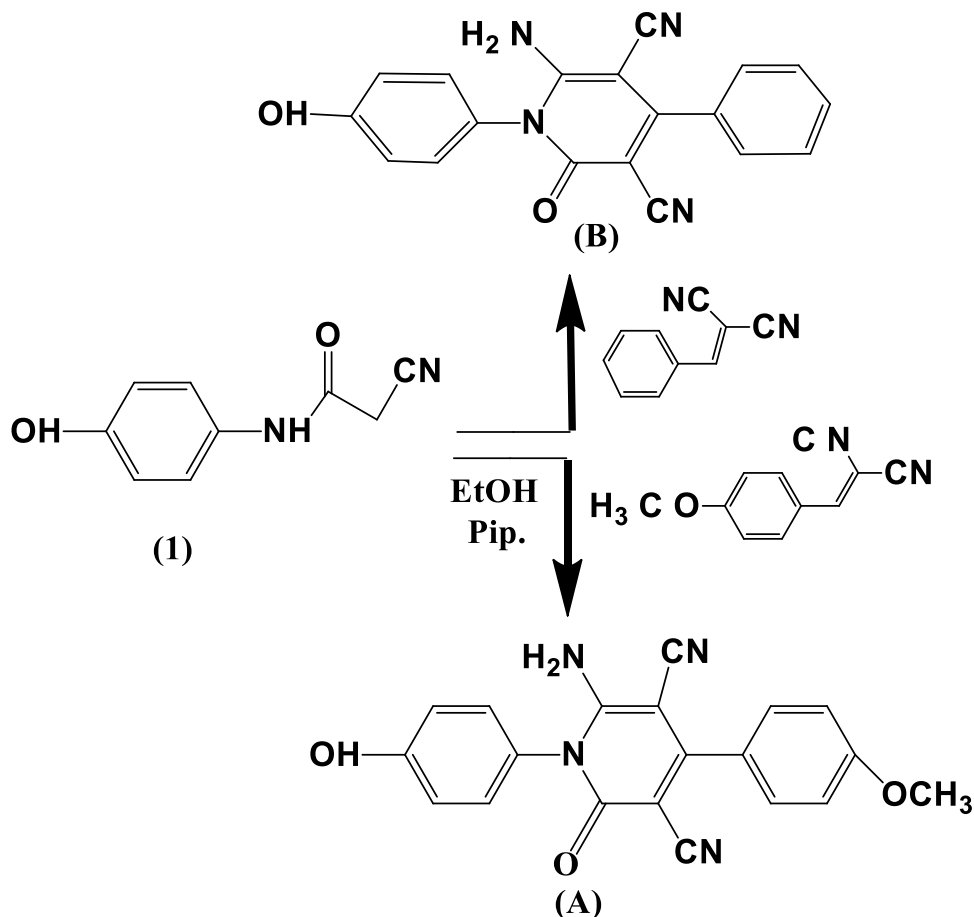
### 2.4 Calculation details

Gaussian 09 W software was used to calculate the DFT. Based on a 6–311 + +G basis set (d, p), the derivatives of pyridone molecules were optimized using the B3LYP method [16]. A detailed analysis of the parameters of quantum chemicals (HOMO and LUMO) was conducted based on the highly and lightly occupied and unoccupied orbitals (HOMO and LUMO) [17]. A Forcite unit from Accelrys Inc. in England was used during the molecular dynamic (MD) simulation. Using a copper box, we simulated and determined its interaction with the adsorbed molecules. This process was carried out in the presence of only one molecule of the inhibitor with 250 molecules of water on the copper surface by adsorption Locator modulus, where the binding energy was calculated through the following equations:

$$E_{interaction} = E_{tot} - (E_{subs} + E_{pyridon}) \quad (3)$$

$$E_{binding} = -E_{interact} \quad (4)$$

**Fig. 1** Synthesis of pyridone derivative compounds (PYR-2 and PYR-3)



$E_{\text{subs}}$  is the total energy of Cu(110) and  $\text{H}_2\text{O}$  molecules,  $E_{\text{pyridone}}$  represents free inhibitor energy, and  $E_{\text{tot}}$  represents the total energy of the whole system.

## 2.5 SEM

The surface of the mechanically polished original Cu sample was identified using SEM and the surface of the Cu samples that had been naturally immersed in the solution for 5 h. Three copper pieces were immersed in hydrochloric acid alone (blank 1M HCl) and another in HCl 1M with  $18 \times 10^{-5}$  M of PYR-2 and the last piece in 1M HCl with  $18 \times 10^5$  M of PYR-3 for 5 hours in this experiment.

## 3 Results and discussion

### 3.1 Structure elucidation of compounds (PYR-2 and PYR-3)

#### 3.1.1 FTIR of compound (PYR-2)

Figure 2 depicts the IR (KBr):  $\nu/\text{cm}^{-1} = 3384$  (OH), 3313 ( $\text{NH}_2$ ), 2216 ( $\text{C}\equiv\text{N}$ ), and 1670 ( $\text{C}=\text{O}$ ).

#### 3.1.2 $^1\text{H}$ NMR of compound (PYR-2)

Figure 3 depicts the  $^1\text{H}$  NMR ( $\text{DMSO}-d_6$ ):  $\delta$  3.85 (s, 3H,  $\text{OCH}_3$ ), 6.91–7.51 (m, 8H, Ar-H), 7.64 (s, 2H,  $\text{NH}_2$ ), and 9.82 (s, 1H, OH).

#### 3.1.3 Mass spectroscopy of compound (PYR-2)

Figure 4 depicts MS  $m/z$  (%): 359 ( $\text{M} + ^+1$ , 17.76), 258 ( $\text{M}^+$ , 37.90), 339 (25.40), 331 (13.73), 313 (16.21), 295 (09.32), 264 (15.81), 105 (19.27), 91 (24.41), 85 (34.25), 55 (78.51), and 43 (100.00).

#### 3.1.4 FTIR analysis of compound (PYR-3)

Figure 5 depicts the IR (KBr):  $\nu/\text{cm}^{-1} = 3380$  (OH), 3305 ( $\text{NH}_2$ ), 2212 ( $\text{C}\equiv\text{N}$ ), and 1672 ( $\text{C}=\text{O}$ ).

#### 3.1.5 $^1\text{H}$ NMR of compound (PYR-3)

$^1\text{H}$  NMR ( $\text{DMSO}-d_6$ ):  $\delta$  6.92–7.57 (m, 9H, Ar-H), 7.79 (s, 2H,  $\text{NH}_2$ ), 9.91 (s, 1H, OH) Fig. 6.

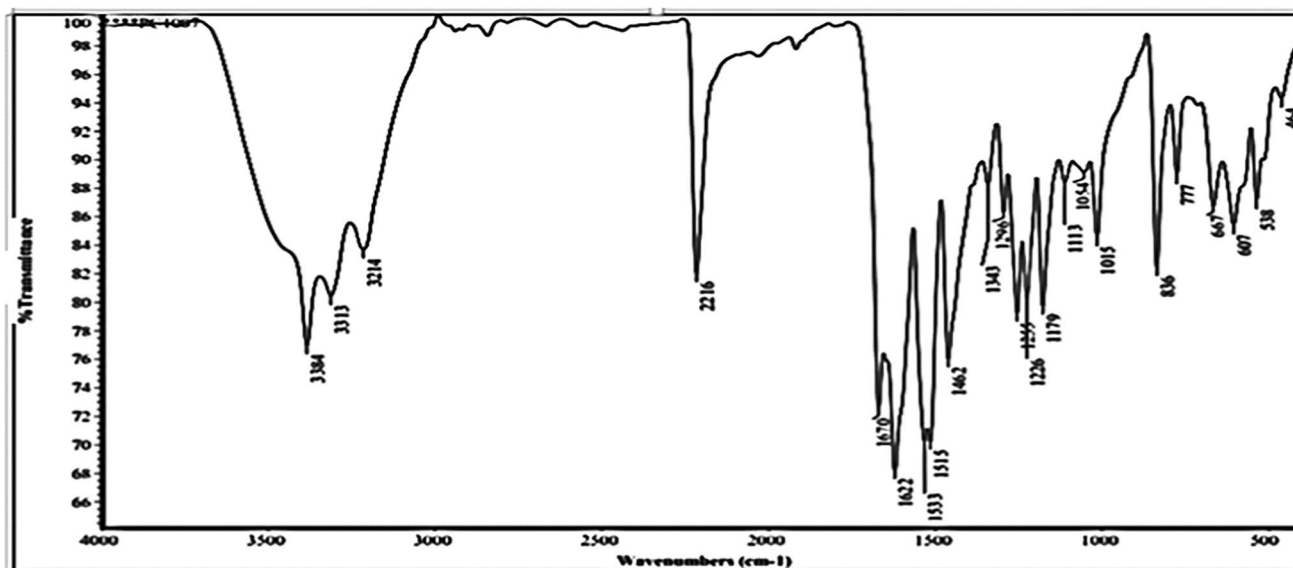


Fig. 2 FTIR spectroscopy of compound PYR-2

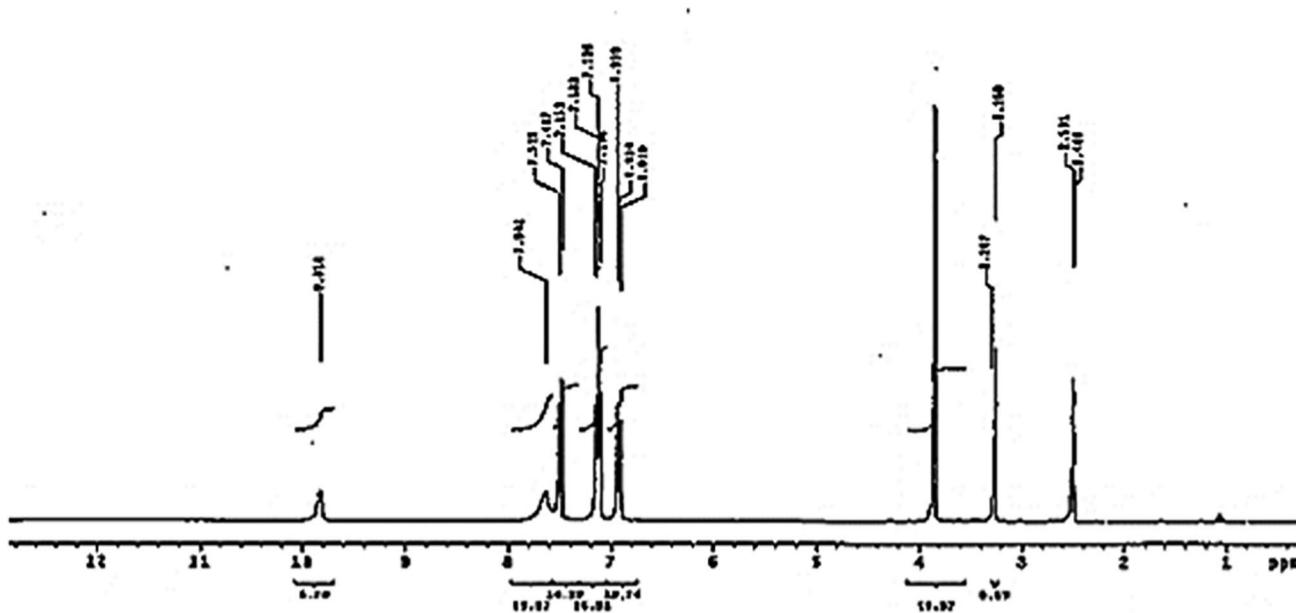


Fig. 3  $^1\text{H-NMR}$  spectrum of compound PYR-2

### 3.1.6 Mass spectroscopy (PYR-3)

MS  $m/z$  (%): 328 ( $M^+$ , 12.75), 310 (18.00), 296 (22.35), 275 (25.78), 262 (33.96), 199 (18.51), 162 (27.43), 119 (42.04), 105 (40.73), and 91 (100.00) Fig. 7.

## 3.2 PP tests

Most PP diagrams between voltage and current assume that inhibitors are adsorbed on the metal's surface to

prevent corrosion. Various concentrations of pyridone derivatives compounds were used to immerse copper in hydrochloric acid for up to 10 min. In Figs. 8 and 9, Tafel diagrams were recorded [18]. At the same time, OCP was stable. Compound PYR-2 exhibited the highest  $\eta\%$ . In Table 1, it was observed that the potential corrosion deviation was less than 85 millivolts, thus proving that the compound is a mixed type [19, 20]. Additionally, the figure showed that the compound worked by preventing hydrogen from spreading on the surface of copper due

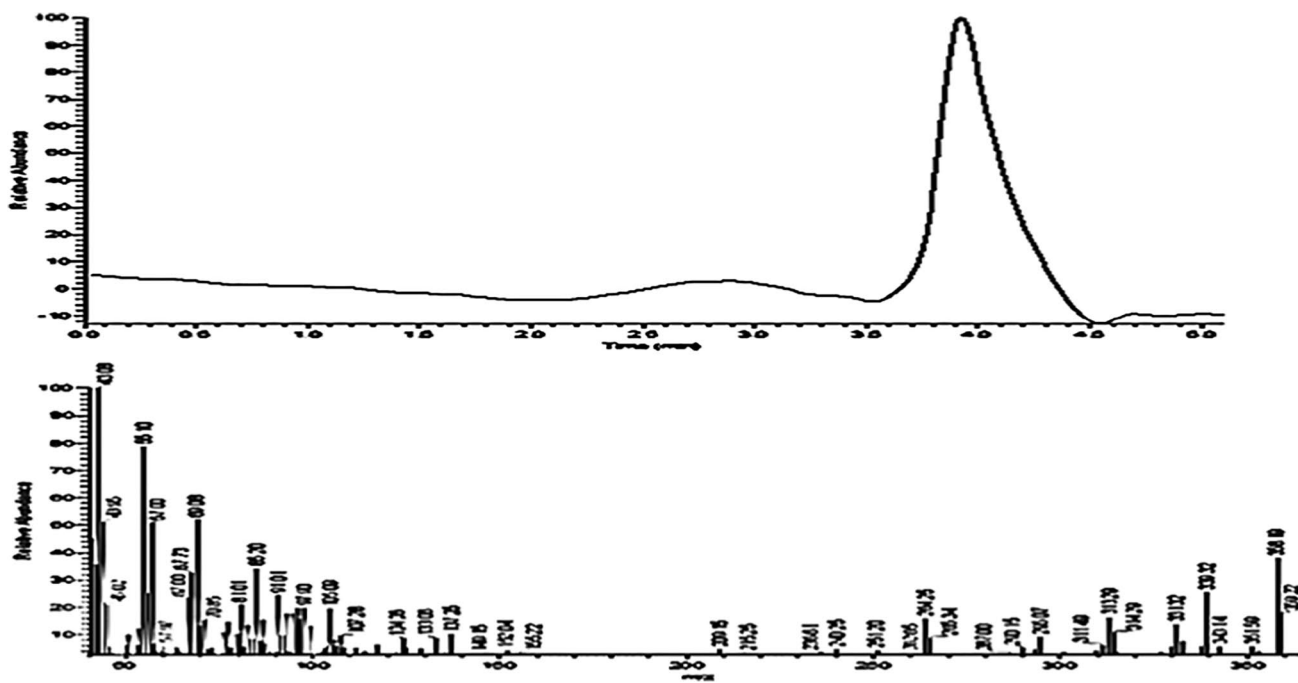


Fig. 4 Mass spectroscopy of compound PYR-2

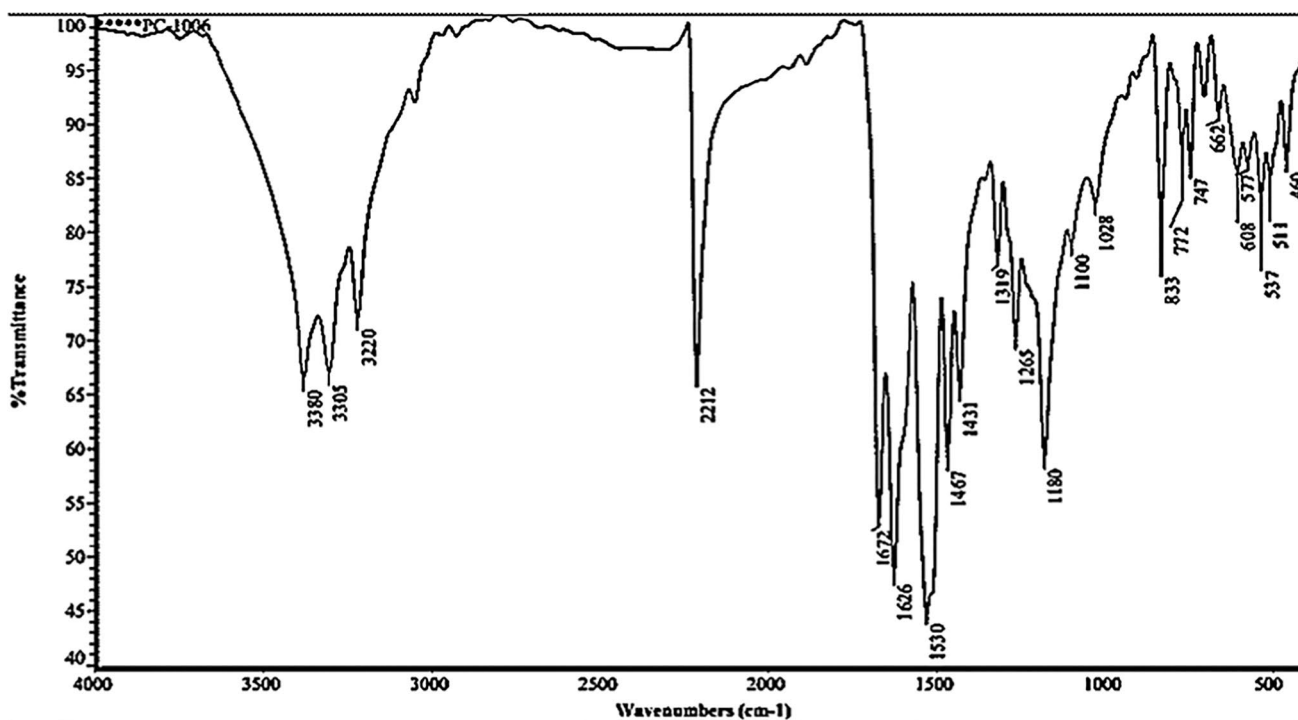


Fig. 5 FTIR spectroscopy of compound PYR-3

to the reaction at the cathode. In addition, these results showed that compound PYR-2 has a more significant effect on inhibiting copper corrosion in HCl than compound PYR-3. According to Figs. 8 and 9, increased

concentrations of pyridone derivatives inhibit the anodic corrosion of Cu electrodes. Moreover, pyridone derivatives suppress cathodic reactions less than anodic reactions when present.  $\beta_a$  values obtained using pyridone



**Fig. 8** Plots of PP of Cu dissolution with and without different doses of compound PYR-2

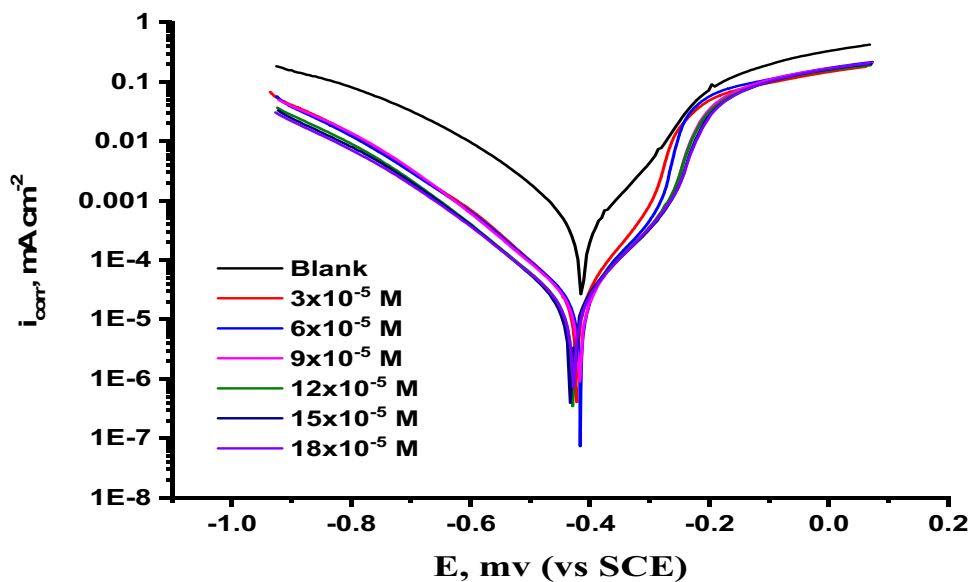
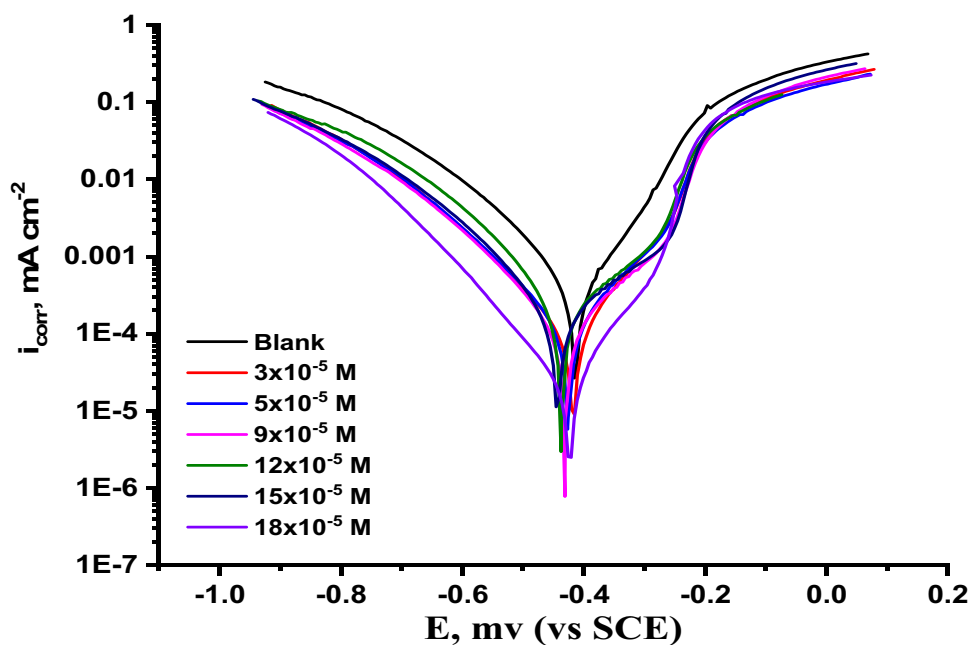


**Fig. 9** Plots of PP of Cu dissolution with and without different doses of compound PYR-3



11, we see that two circles are incomplete: The first one was related to charging transfer at high frequencies, while the other was due to the formation of the adsorbed layer on copper from pyridone derivatives at low frequencies, appearing as a large ring [22]. A solution of chlorinated ions diffuses towards the positive copper electrode, forming  $[CuCl^-]$ ,  $[CuCl_2^-]$ , and then the obstruction is gradually dissolved when pyridone derivatives are added. Adding pyridone derivatives gradually increases the loop's radius, as does add more pyridone derivatives [23]. There was a significant reduction in the migration of negative chloride ions on the copper surface owing to forming of

a pyridone derivatives layer on the copper surface. Also, double layer capacitance ( $C_{dl}$ ) was computed by employing the equation:

$$C_{dl} = Y_o(2\pi f_{max})^{n-1} \tag{5}$$

$Y_0$  and  $f_{max}$  are the CPE and frequency magnitude at which the imaginary component of the impedance reaches the maximum value, respectively. In  $n = \alpha/(\pi/2)$ ,  $n$  is an adjustable factor, and  $\alpha$  is the phase angle [24, 25].  $C_{dl}$  equivalents which appear in Tables 2 and 3, decrease with increasing pyridone derivative doses, which can be attributed to either a decrease in the dielectric constant value

**Table 1** PP parameters of Cu in 1 M HCl in the lack and existence of numerous doses of compounds PYR-2 and PYR-3

Comp	Conc. $\times 10^{-5}$ M	$i_{\text{corr}}$ , $\mu\text{A cm}^{-2}$	$E_{\text{corr}}$ , mV vs. SCE	$\beta_a$ mV dec $^{-1}$	$\beta_c$ mV dec $^{-1}$	C.R mpy	$\Theta$	% IE
Blank	0.0	494.0	413	123	181	131	—	—
PYR-2	3	115.0	423	125	190	47	0.767	76.7
	6	102.0	431	121	181	35	0.794	79.4
	9	78.0	421	119	183	31	0.842	84.2
	12	62.0	423	120	189	28	0.874	87.4
	15	55.0	418	121	181	23	0.889	88.9
	18	40.0	420	119	192	20	0.919	91.9
PYR-3	3	125.0	420	118	173	65	0.747	74.7
	6	112.0	423	116	186	51	0.773	77.3
	9	88.0	422	120	196	41	0.822	82.2
	12	69.0	425	123	184	38	0.860	86.0
	15	58.0	420	122	181	31	0.883	88.3
	18	48.0	425	121	187	29	0.903	90.3

**Fig. 10** The Nyquist (a) and bode (b) plots for dissolution of Cu in 1.0 M HCl without and with various doses of the compound PYR-2

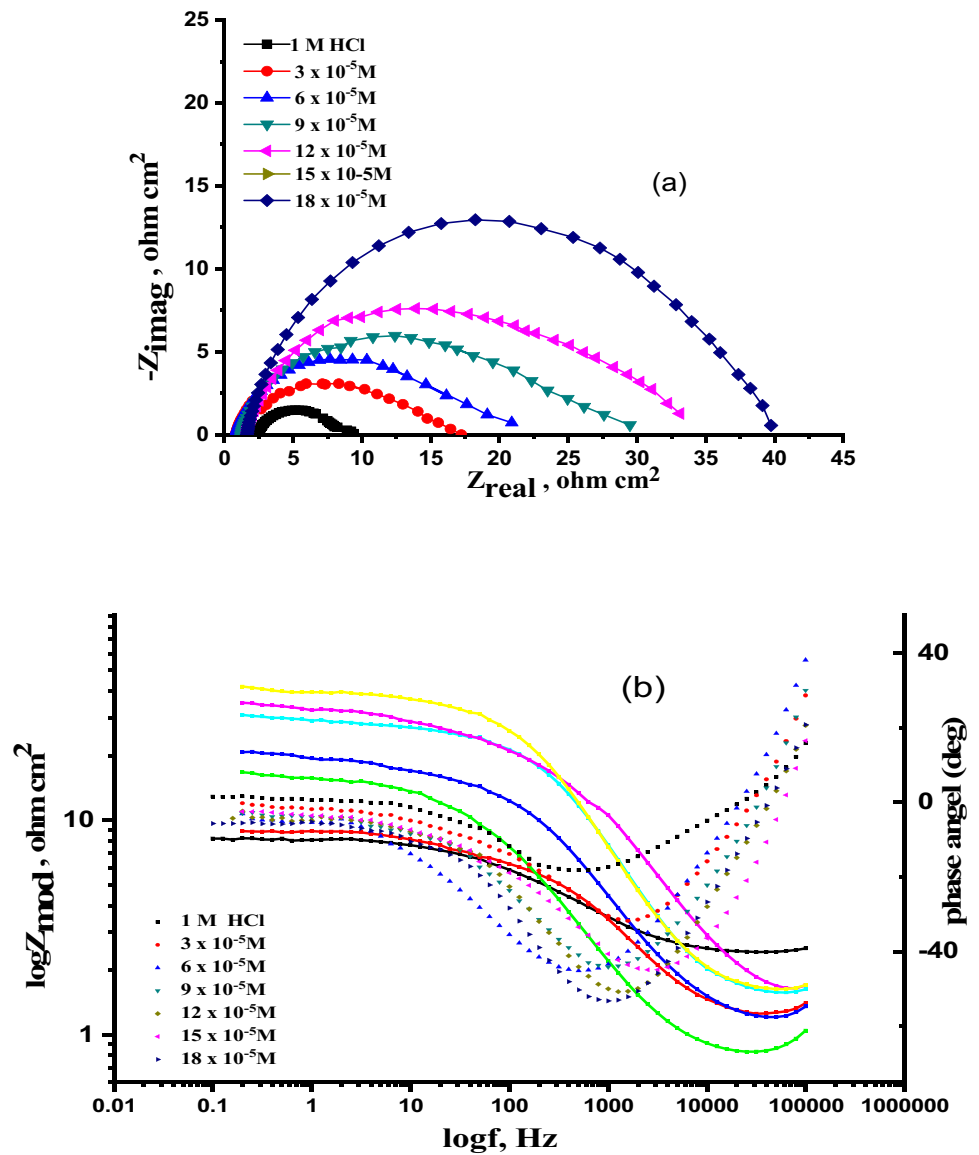




**Fig. 11** The Nyquist (a) and bode (b) plots for dissolution of Cu in 1.0 M HCl without and with various doses of the compound PYR-3

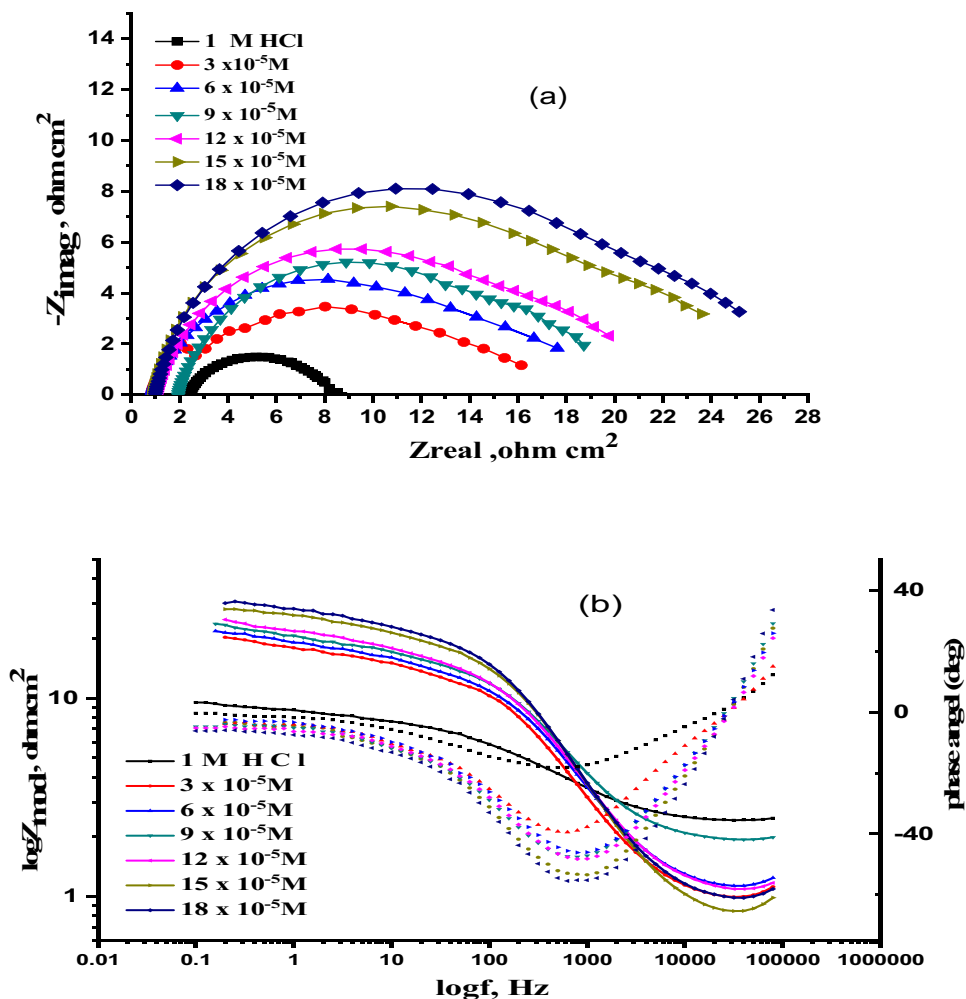


**Table 2** EIS data for the corrosion of Cu in 1.0 M HCl in the lack and existence of numerous doses of compound PYR-2

Inhibitor A, M	$C_{dl} \times 10^5, F\ cm^{-2}$	$R_{ct}, \Omega\ cm^2$	$\theta$	% IE
Blank	438.0	5.44	--	--
$3 \times 10^{-5}$	7.45	6.73	0.192	19.2
$6 \times 10^{-5}$	6.51	13.65	0.601	60.1
$9 \times 10^{-5}$	5.64	15.51	0.649	64.9
$12 \times 10^{-5}$	5.24	24.61	0.779	77.9
$15 \times 10^{-5}$	4.82	27.41	0.801	80.1
$18 \times 10^{-5}$	3.01	34.50	0.842	84.2

**Table 3** EIS data for the corrosion of Cu in 1 M HCl in the lack and existence of numerous doses of compound PYR-3

Inhibitor B, M	$C_{dl} \times 10^5, F\ cm^{-2}$	$R_{ct}, \Omega\ cm^2$	$\theta$	% IE
Blank	438	5.44	-	-
$3 \times 10^{-5}$	5.60	23.23	0.766	76.6
$6 \times 10^{-5}$	3.70	33.51	0.838	83.8
$9 \times 10^{-5}$	3.49	40.16	0.864	86.4
$12 \times 10^{-5}$	3.33	67.62	0.920	92.0
$15 \times 10^{-5}$	2.50	90.49	0.940	94.0
$18 \times 10^{-5}$	1.83	128.40	0.958	95.8

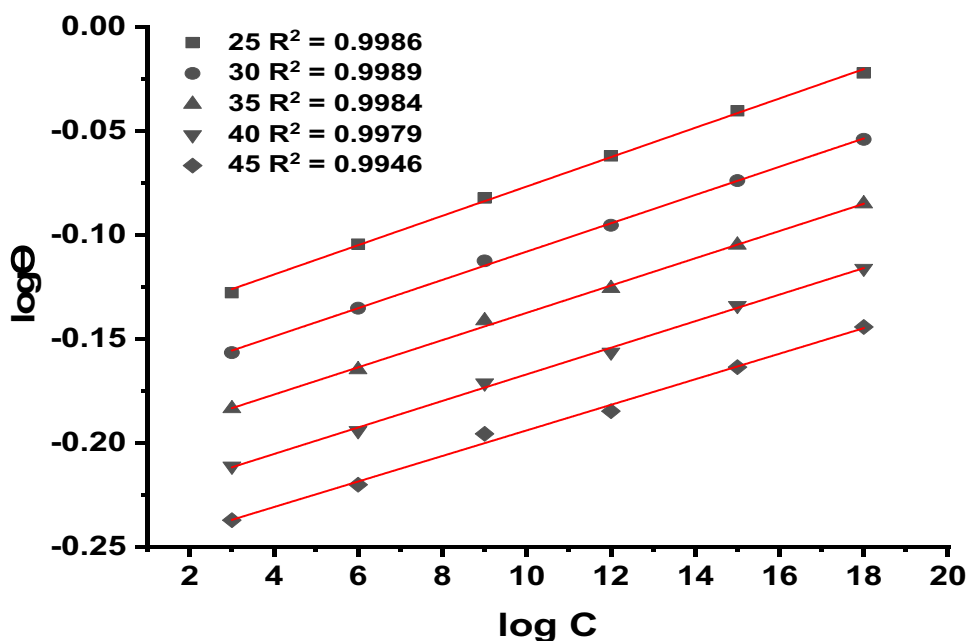
or to the double layer or to the adsorption layer, which has become, to a large extent, thick.

### 3.4 Adsorption isotherm

We need to do adsorption isotherms to understand why copper is affected by the inhibitor on its surface. In testing several isotherms for pyridone compounds adsorbing on copper

surfaces, we found that the Freundlich isotherm fitted the best [26]. ACR-2 and ACR-3 molecules adsorb in 1.0 M HCl solutions with correlation coefficients and slopes close to 1, indicating Freundlich adsorption isotherms. The  $K_{ads}$  values could be determined from the intersections of the lines on the  $\Theta$ -axis, and  $K_{ads}$  was related to the standard free energy of adsorption  $\Delta G^0_{ads}$ . The quantity of material adsorbed ( $\Theta$ ) is linked to the dose (C) by the equation:

**Fig. 12** Freundlich isotherm for the compound A on Cu surface in 1 M HCl at various temperatures



$$\theta = kC^n \quad (6)$$

The plot of  $\log \theta$  versus  $\log C$  is a straight line with 'n' as the slope which depicts in Fig. 12; the free energy of adsorption  $\Delta G_{\text{ads}}^{\circ}$  for numerous doses of inhibitor at various temperatures was computed by employing the equation:

$$\Delta G_{\text{ads}}^{\circ} = -RT \ln(55.5 \times K) \quad (7)$$

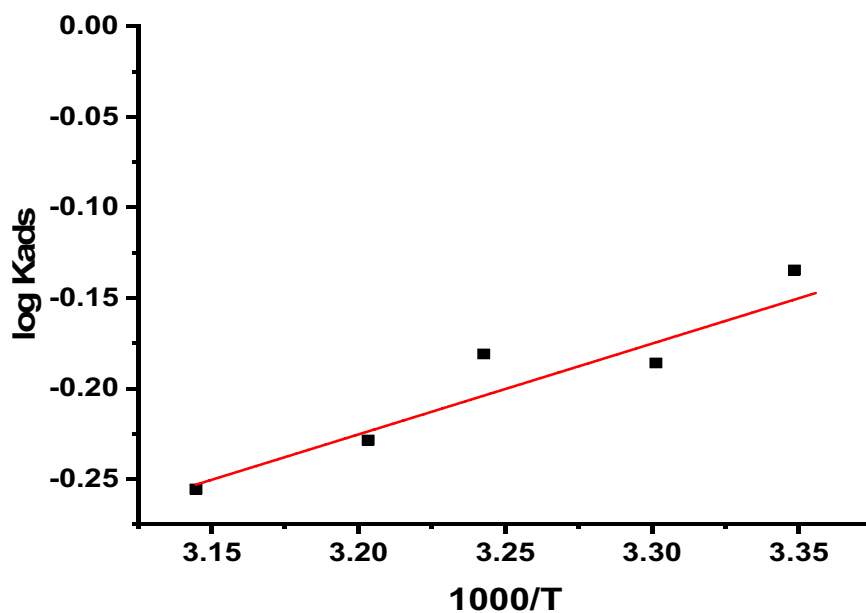
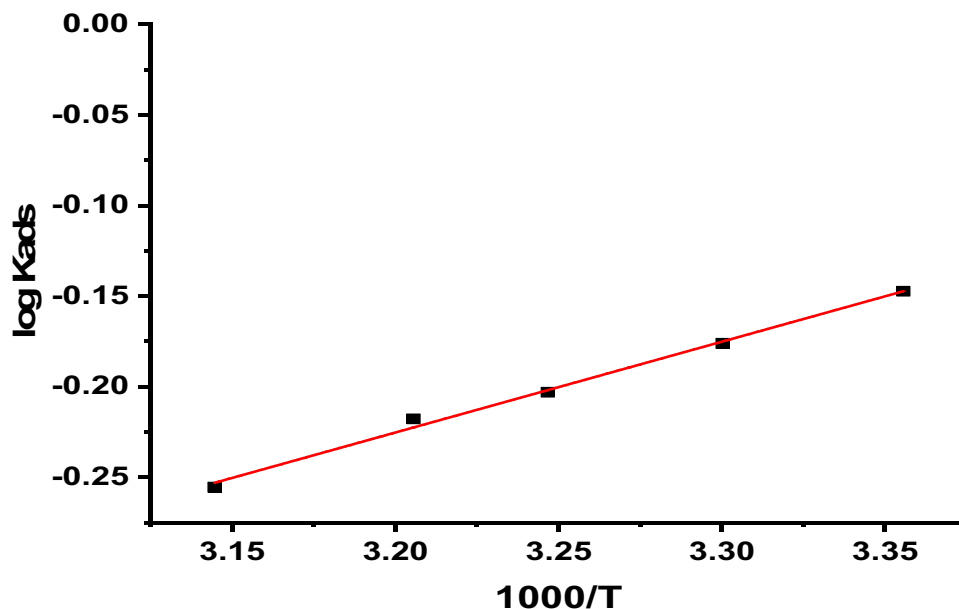
In  $K = \theta/C(1-\theta)$ ,  $\theta$  is surface coverage, and  $C_{\text{inh}}$  is the dose of inhibitor.

The literature shows that the value of  $\Delta G_{\text{ads}}^{\circ}$  every time it is higher than  $-20$  kJ/mol or less negative means that the charges are attracted and the inhibitor was adsorbed physically to the surface [27]. The difference between the two, if it is more negative than  $-40$  kJ/mol, means that the inhibitor is chemically adsorbing onto the surface of Cu [28]. The value of  $\Delta G_{\text{ads}}^{\circ}$  for inhibitor PYR-2 is  $-16.3$  kJ/mol and inhibitor PYR-3 is  $-13.2$  kJ/mol, indicating that two inhibitors were physically adsorbed on the copper surface and the reaction is spontaneous. Figure 13 indicates the relation between  $\log k_{\text{ads}}$  on y-axis and  $1000/T$  on x-axis which calculated the  $\Delta H$  from the slope. Also, the reaction is exothermic because the  $\Delta H$  value is negative [29]. The enthalpy values resulting from electrostatic interactions between charged molecules and charged metal (physisorption) range up to  $41.9$  kJ mol $^{-1}$ , whereas those, resulting from chemisorption, range up to about  $100$  kJ mol $^{-1}$ . Physisorption produces molecules with small absolute enthalpy values. In the presence of the investigated compounds,  $\Delta S_{\text{ads}}^{\circ}$  values are large and negative, indicating the increase in the ordering on the copper surface [30, 31].

### 3.5 Molecular modeling

Figure 14 depicted the optimized structure, electrostatic potential (ESP) map, and HOMO and LUMO density distributions of PYR-2 and PYR-3, respectively. In HOMO sites, the red color represents a high electron density; while in LUMO sites, the green color represents a low electron density. Having a high electron density allows the metal surface to donate electrons. Electrons are received by the metal surface in the green area [6]. This means that it is extremely important to consider how these two areas are distributed. For testing the effect of molecular structure on the performance of corrosion inhibitors, DFT was used to obtain optimized molecular geometries. A molecule model was developed using Gauss View 2009, and a DFT calculation was performed using the basis set 6-31G (d). A detailed calculation method is described elsewhere, including quantum chemical parameters [32, 33]. The electron-donating properties of molecules and surfaces play a significant role in understanding how inhibitors interact with metallic surfaces. Dipole moments are used to measure the polarity of molecules. Their polar functional groups interact with metal surfaces, causing inhibitor molecules to adsorb on them [34]. The ESP map shows the electrophilic and nucleophilic activity corresponding to the positive and negative regions. In theory, the metal acts as an electrophilic agent, creating strong covalent bonds between the atoms of the inhibitor, especially those containing heterogeneous atoms and those with electronegative and nucleophilic centers [35]. Compound PYR-2 can easily form covalent bonds to the copper surface, as shown in the (ESP) map, because the positive and negative zones

**Fig. 13** Plot of variation of Log  $K_{ads}$  vs.  $1000/T$  for the adsorption of numerous doses of compounds PYR-2 and PYR-3 on the Cu surface in 1 M HCl at various temperatures



are deeper in compound PYR-2. As we noted in Table 4, we also measured  $E_{HOMO}$  and  $E_{LUMO}$  values, which tell us whether the compound can give or receive electrons [36]. As we can see from the table, compound 1 has a greater  $E_{HOMO}$  value than compound PYR-3, suggesting that compound PYR-2 is better able to give electrons off than compound PYR-3, which implies that it will adsorb more on copper's surface [37]. A lower energy gap ( $\Delta E$ ) value in compound 1 than in compound PYR-3 indicates that compound PYR-2 is more chemically active on copper than compound PYR-3.

### 3.6 MD simulation

To gain a deeper understanding of how inhibition works, we simulated between pyridone compounds and copper surfaces. Figure 15 shows the adsorption of compounds 1 and 2 formed on Cu. Figure 15 shows how compounds adsorb on copper's surface horizontally, allowing electrons to move easily, forming covalent bonds, and increasing the binding energy between the compounds and copper [38, 39]. The adsorption energy value for compound PYR-2 is  $-3050.8$  but is  $-3041.2$  for compound PYR-3,

**Fig. 14** Optimized structure, HOMO, LUMO, and ESP map of compounds A and B

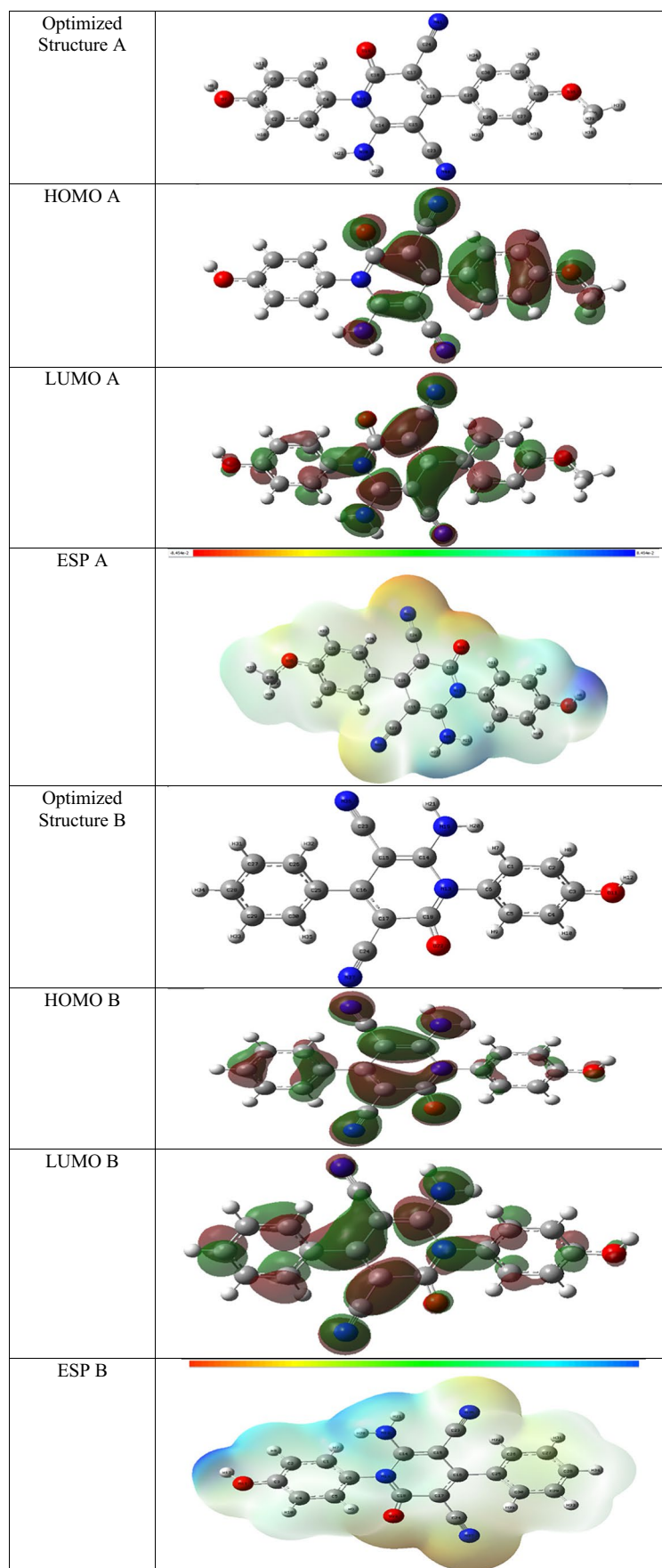


**Table 4** Quantum parameters of compounds PYR-2 and PYR-3

Compound	$E_{HOMO}$	$E_{LUMO}$	$\Delta E$	Dipole moment
PYR-2	-5.866	-1.837	4.029	7.4156
PYR-3	-6.140	-1.965	4.175	8.7868

indicating compound 1 inhibits the corrosion of Cu in 1.0 M HCl. Pyridone compounds and negative  $E_{ads}$  indicate a strongly adsorbed Cu substrate. A greater amount of adsorption energy is obtained when Cu is diluted with HCl, making pyridone compounds more effective in

protecting Cu. According to this theoretical analysis, all available data are accurate and support previous studies. Lastly, pyridone inhibitors offer great protection against corrosion. PYR-2 and PYR-3  $E_{ads}$  negative indicate that strong and spontaneous adsorption occurred on the copper substrate [40]. The results of Table 5 indicate that PYR-2 has greater adsorption energy than PYR-3, indicating it will perform better as an inhibitor for the protection of copper in 1.0 M HCl than PYR-3. This theoretical analysis supports previous studies and is accurate for all available data. Lastly, PYR-2 and PYR-3 inhibitors offer great protection against corrosion.

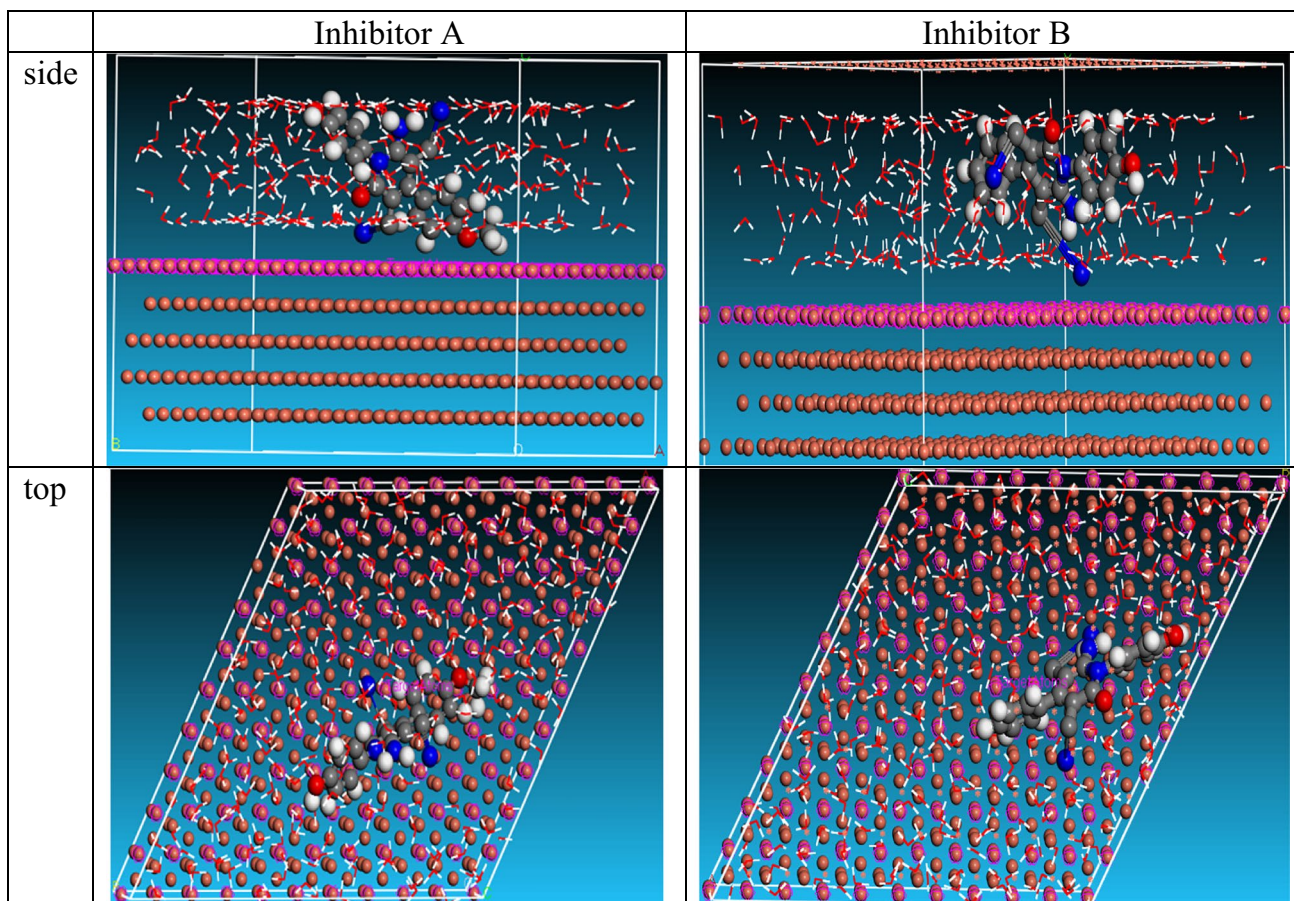
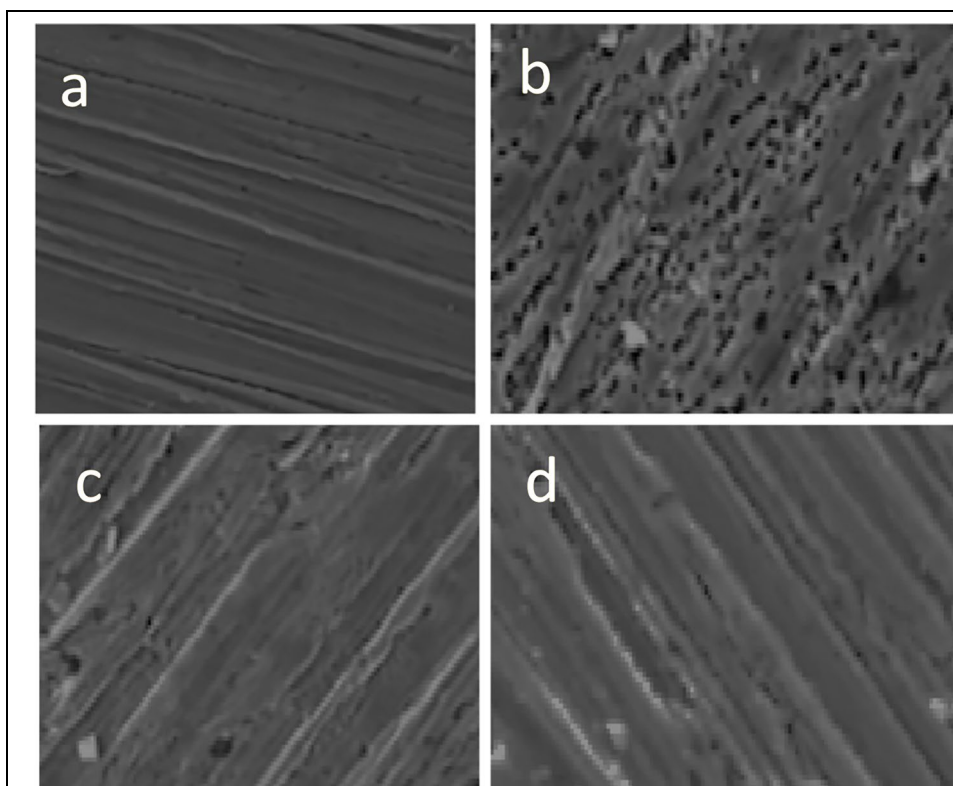


**Fig. 15** Adsorption of pyridone compounds on Cu surface

**Table 5** Monte Carlo simulation parameters of adsorption of pyridone e compounds on Cu surface

Structure	Total energy	Adsorption energy	Rigid adsorption energy	Deformation energy	$E_{ads}$ : pyridone e	$E_{ads}$ : water
Cu (1 1 1)–1 Inhibitor PYR-2	-3198.9	-3050.8	-3262.8	211.9	-121.3	-13.3
Cu (1 1 1)–1 Inhibitor PYR-3	-3191.5	-3041.2	-3254.7	213.4	-118.5	-14.3

**Fig. 16** SEM images from Cu **a** before and **b** after soaking time for 1 h in the blank, and **c** in the  $18 \times 10^{-5}$  M inhibitor PYR-2 **d** in the  $18 \times 10^{-5}$  M inhibitor PYR-3 for 5 h

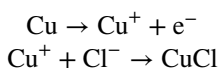


### 3.7 SEM analysis

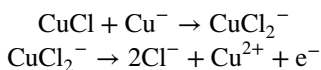
The surface characteristics investigation (SEM) for the Cu coupons immersed for 5 h in a solution of 1.0 M HCl solution in the lack and existence of the optimum concentration ( $18 \times 10^{-5}$  M) of inhibitor 1 has been postulated in Fig. 16. From the SEM images as in Fig. 16a, it can be seen that the significant damage on the Cu surface was fulfilled with the corrosion product while, in Fig. 16b and c, after adding the optimum concentration of inhibitor 1, the Cu surface became more smooth [41, 42].

### 3.8 Mechanism of inhibition

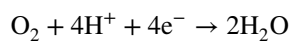
The following reaction illustrates the mechanism of copper degradation at the anode:



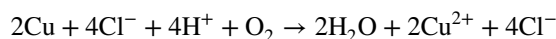
Then,  $\text{Cl}^-$  reacts with CuCl to form soluble  $\text{CuCl}_2^-$ .



The cathodic reaction in HCl occurs by the following reaction:



Thus, Cu overall corrosion reaction in HCl is:



This study suggests that the protonation of the  $\text{NH}_2$  on the investigated pyridone may have led to its solubility in water. Protonated compounds, however, can interact with metals through electrostatic interaction. It is also possible that pyridone could interact with d orbitals of Cu metal by lone pair  $\text{e}^-$  in O and N, or aromatic rings  $\pi \text{e}^-$  of Cu could also donate an electron to the vacant antibonding orbital of inhibitor molecules (reterodonation).

## 4 Conclusion

Experimental experiments proved the effectiveness of pyridone derivatives in inhibiting copper corrosion in 1.0 M HCl solution as mixed type inhibitors. A Langmuir adsorption isotherm was observed for these compounds upon adsorption onto copper surfaces, which correlated with the inhibition process. The presence of a negative value for  $\Delta G_{\text{ads}}^0$  indicates spontaneity in the reaction. PYR-2 and PYR-3 exhibited increased inhibition strength when electrons were donated and gained from high-occupied orbitals (HOMO)

to low-occupied orbitals (LUMO). The corrosion process depends on the relative ability of the compounds to donate electrons to the metal. In the end, the results were found to agree with the measurements. This study presents the possibility of using the economically and effectively protect Cu by pyridone inhibitors in HCl solution in the future.

**Author contributions** This work has been done by Badreah A. Al Jahdaly.

**Data availability** The author confirms that the data supporting this study are available within the article.

## Declarations

**Ethical approval** Not applicable.

**Competing interests** The author declares no competing interests.

## References

- Dobkowska A et al (2021) A comparison of the corrosion behaviour of copper materials in dilute nitric acid. *Corros Sci* 192:109778
- Fouda A, Elabbasy H (2019) Corrosion inhibition effect of methanol extract of nerium oleander on copper in nitric acid solutions. *Int J Electrochem Sci* 14:6884–6901
- Fouda A, Haleem EA (2018) Berry leaves extract as green effective corrosion inhibitor for Cu in nitric acid solutions. *Surf Eng Appl Electrochem* 54(5):498–507
- El Basiony N et al (2021) Synthesis, characterization, theoretical calculations (DFT and MC), and experimental of different substituted pyridine derivatives as corrosion mitigation for X-65 steel corrosion in 1M HCl. *J Mol Struct* 1231:129999
- Khaled MA et al (2021) Novel pyrimidine-bichalcophene derivatives as corrosion inhibitors for copper in 1 M nitric acid solution. *RSC Adv* 11(41):25314–25333
- Motawea M, El-Hossiany A, Fouda A (2019) Corrosion control of copper in nitric acid solution using chenopodium extract. *Int J Electrochem Sci* 14:1372–1387
- El-Haitout B et al (2023) Exploring the feasibility of new eco-friendly heterocyclic compounds for establishing efficient corrosion protection for N80 steel in a simulated oil well acidizing environment: from molecular-level prediction to experimental validation. *Colloids Surf, A* 656:130372
- Verma C, Quraishi M, Rhee KY (2021) Present and emerging trends in using pharmaceutically active compounds as aqueous phase corrosion inhibitors. *Journal of Molecular Liquids*, 328:115395
- Gorobets NY et al (2004) Rapid microwave-assisted solution phase synthesis of substituted 2-pyridone libraries. *Tetrahedron* 60(39):8633–8644
- Fujita Y, Oguri H, Oikawa H (2005) Biosynthetic studies on the antibiotics PF1140: a novel pathway for a 2-pyridone framework. *Tetrahedron Lett* 46(35):5885–5888
- Li Q, Mitscher LA, Shen LL (2000) The 2-pyridone antibacterial agents: bacterial topoisomerase inhibitors. *Med Res Rev* 20(4):231–293
- Parlow JJ et al (2003) Design, synthesis, and crystal structure of selective 2-pyridone tissue factor VIIa inhibitors. *J Med Chem* 46(22):4696–4701
- Hasvold LA et al (2003) Pyridone-containing farnesyltransferase inhibitors: synthesis and biological evaluation. *Bioorg Med Chem Lett* 13(22):4001–4005
- Fouda A et al (2020) Synthesis, characterization, and application of new nonionic surfactant as a corrosion inhibitor for carbon steel in 1 M hydrochloric acid solution. *J Bio-and Tribo-Corrosion* 6(3):1–9
- Fouda A et al (2019) Calicotome extract as a friendly corrosion inhibitor for carbon steel in polluted NaCl solution: chemical and electrochemical studies. *Egypt J Chem* 62(10):1879–1894
- Fouda A, Wahba A, Al-Bonayan AM (2021) Corrosion inhibition of stainless steel in 1.0 M hydrochloric acid solution using novel nonionic surfactant: electrochemical and density functional theory/B3LYP/6–31G\* analysis. *Surf Eng Appl Electrochem* 57(6):689–702
- Cassidy J et al (2018) High-performance, robustly verified Monte Carlo simulation with FullMonte. *J Biomed Opt* 23(8):085001
- Fouda A, Etaiw S, Wahba A (2015) Effect of acetazolamide drug as corrosion inhibitor for carbon steel in hydrochloric acid solution. *Nat Sci* 13(9):1–8
- Aziz I et al (2022) Corrosion inhibition potential of a new corrosion inhibitor for mild steel in 1 M hydrochloric acid solution determined by weight loss technique, complemented with adsorption studies and DFT calculations. *Int J Corros Scale Inhib* 11(1):64–81
- About S et al (2021) Gravimetric, electrochemical and theoretical study, and surface analysis of novel epoxy resin as corrosion inhibitor of carbon steel in 0.5 M H<sub>2</sub>SO<sub>4</sub> solution. *Journal of Molecular Structure*, 1245: 131014
- Zhang W et al (2021) Chemically modified resveratrol as green corrosion inhibitor for Q235 steel: electrochemical, SEM, UV and DFT studies. *J Mol Liq* 343:117672
- Vengatesh G, Sundaravadivelu M (2019) Non-toxic bisacodyl as an effective corrosion inhibitor for mild steel in 1 M HCl: thermodynamic, electrochemical, SEM, EDX, AFM, FT-IR, DFT and molecular dynamics simulation studies. *J Mol Liq* 287:110906
- Abd El-Raouf M et al (2018) Electrochemical and quantum chemical evaluation of new bis (coumarins) derivatives as corrosion inhibitors for carbon steel corrosion in 0.5 M H<sub>2</sub>SO<sub>4</sub>. *J Mol Liq* 255:341–353
- Benali O et al (2021) Carbon steel corrosion inhibition in H<sub>2</sub>SO<sub>4</sub> 0.5 M medium by thiazole-based molecules: weight loss, electrochemical, XPS and molecular modeling approaches. *Colloids Surf A: Physicochem Eng Aspects* 630:127556
- Habeeb HJ et al (2018) Development of new corrosion inhibitor tested on mild steel supported by electrochemical study. *Results Phys* 8:1260–1267
- Fouda A, El-Awady G, El Behairy W (2018) Prosopis juliflora plant extract as potential corrosion inhibitor for low-carbon steel in 1 M HCl solution. *J Bio-and Tribo-Corrosion* 4(1):8
- Hsissou R et al (2020) Development and potential performance of prepolymer in corrosion inhibition for carbon steel in 1.0 M HCl: outlooks from experimental and computational investigations. *J Colloid Interface Sci* 574:43–60
- Sliem MH et al (2019) AEO7 surfactant as an eco-friendly corrosion inhibitor for carbon steel in HCl solution. *Sci Rep* 9(1):1–16
- Iroha NB et al (2022) Evaluation of the anticorrosion performance of Tamsulosin as corrosion inhibitor for pipeline steel in acidic environment: experimental and theoretical study. *J Taibah Univ Sci* 16(1):288–299
- Abu-Rayyan A et al (2022) A study of the synthesis and characterization of new acrylamide derivatives for use as corrosion inhibitors in nitric acid solutions of copper. *Nanomaterials* 12(20):3685

31. Alwi MAM et al (2022) Gravimetric and electrochemical statistical optimizations for improving copper corrosion resistance in hydrochloric acid using thiosemicarbazone-linked 3-acetylpyridine. *RSC Adv* 12(43):27793–27808
32. Su L et al (2021) Regulating local electron density of iron single sites by introducing nitrogen vacancies for efficient photo-Fenton process. *Angew Chem Int Ed* 60(39):21261–21266
33. Tang S et al (2012) Highly efficient deep-blue electroluminescence based on the triphenylamine-cored and peripheral blue emitters with segregative HOMO–LUMO characteristics. *J Mater Chem* 22(10):4401–4408
34. Madkour LH, Elroby S (2015) Inhibitive properties, thermodynamic, kinetics and quantum chemical calculations of polydentate Schiff base compounds as corrosion inhibitors for iron in acidic and alkaline media. *Int J Ind Chem* 6(3):165–184
35. Cerón ML et al (2020) Computing the Fukui function in solid-state chemistry: application to alkaline earth oxides bulk and surfaces. *J Phys Chem A* 124(14):2826–2833
36. Lin S-S et al (2020) Approach based on TOPSIS and Monte Carlo simulation methods to evaluate lake eutrophication levels. *Water Res* 187:116437
37. Khadom AA et al (2022) Influence of apricot constituents as eco-friendly corrosion inhibitor for mild steel in acidic medium: a theoretical approach. *J Mol Liq* 347:117984
38. Santhy K et al (2019) Molecular structure, spectroscopic (FT-IR, FT-Raman) studies, Homo-Lumo and Fukui function calculations of 2-Acetyl amino-5-bromo-4 methyl pyridine by density functional theory. *Chem Data Collect* 24:100291
39. Chen S et al (2020) Camphor leaves extract as a neoteric and environment friendly inhibitor for Q235 steel in HCl medium: combining experimental and theoretical researches. *J Mol Liq* 312:113433
40. Salem A et al (2022) Experimental and computational chemical studies on the corrosion inhibitive properties of metamizole sodium pharmaceutical drug compound for CS in hydrochloric acid solutions. *J Indian Chem Soc* 99(12):100778
41. Hamidah I et al (2021) Corrosion of copper alloys in KOH, NaOH, NaCl, and HCl electrolyte solutions and its impact to the mechanical properties. *Alex Eng J* 60(2):2235–2243
42. Sait N et al (2022) Electrochemical investigation of di-phosphonic acid on corrosion inhibition behavior of copper in hydrochloric acid medium. *J Iran Chem Soc* 19(2):463–473

**Publisher's note** Springer Nature remains neutral with regard to jurisdictional claims in published maps and institutional affiliations.

Springer Nature or its licensor (e.g. a society or other partner) holds exclusive rights to this article under a publishing agreement with the author(s) or other rightsholder(s); author self-archiving of the accepted manuscript version of this article is solely governed by the terms of such publishing agreement and applicable law.